Implicit Brain Imaging

Facundo Mémoli * **Guillermo Sapiro**† **Paul Thompson**‡

Abstract

We describe how implicit surface representations can be used to solve fundamental problems in brain imaging. This kind of representation is not only natural following the state-of-the-art segmentation algorithms reported in the literature to extract the different brain tissues, but it is also, as shown in this paper, the most appropriate one from the computational point of view. Examples are provided for finding constrained special curves on the cortex, such as sulcal beds, regularizing surface based measures, such as cortical thickness, and for computing warping fields between surfaces such as the brain cortex. All these result from efficiently solving partial differential equations and variational problems on surfaces represented in implicit form. The implicit framework avoids the need to construct intermediate mappings between 3D anatomical surfaces and parametric objects such planes or spheres, a complex step that introduces errors and is required by many other cortical processing approaches.

1 Introduction

Some of the most fundamental brain imaging analysis processes can be seen as finding appropriate maps from a general manifold $\mathcal{M}$ (*domain manifold*) onto another general manifold $\mathcal{N}$ (*target manifold*). For example, to compare brain data across subjects, individual brain datasets ($\mathcal{M}$) are often mapped to a neuroanatomical template or brain atlas ($\mathcal{N}$), using a spatial transformation that deforms brain surfaces or volumes to match their counterparts in the atlas, e.g., [4, 17, 71]. Additional examples are finding special curves such as sulcal beds ($\mathcal{M}$ being a segment of the real line and $\mathcal{N}$ the 3D brain surface, i.e., the cortex), regularizing or smoothing maps of surface-based signals, such as fMRI data (see paper by Faugeras *et al.* in this issue) or cortical thickness ($\mathcal{M}$ being the 3D brain surface and $\mathcal{N}$ the positive real line), and brain warping (both $\mathcal{M}$ and $\mathcal{N}$ are 3D brains), e.g., [12, 53, 71]. In other words, it is fundamental for brain imaging research to efficiently compute maps between manifolds, from a generic $\mathcal{M}$ to a generic $\mathcal{N}$. Moreover, all these important tasks can be addressed with partial differential equations (PDEs) or variational formulations between the two manifolds. PDEs have been widely used in neuroimaging, for example in segmenting anatomy using deformable surfaces and probability diffusion [9, 19, 42, 68], in denoising or enhancing brain-derived signals using anisotropic diffusion or scale-spaces [80], and in computing structural brain changes in development or dementia, e.g., [26, 27, 69] and references therein. In this paper, we review and extend work developed in [8, 48, 50] to show that when the cortical surface of the brain is represented in implicit form (defined below), these fundamental brain imaging operations are not only simplified, but they also avoid ad-hoc intermediate projections of the data to planar or spherical coordinate systems, e.g., [3, 25, 75, 82, 60], that can degrade the accuracy of the results. The key idea behind the techniques described

*Electrical and Computer Engineering, University of Minnesota, Minneapolis, MN 55455, memoli@ece.umn.edu.

†Corresponding author: Electrical and Computer Engineering and Digital Technology Center, University of Minnesota, Minneapolis, MN 55455, guille@ece.umn.edu

‡Laboratory of Neuro Imaging, UCLA School of Medicine, Los Angeles, CA 90095, thompson@loni.ucla.edu

here is to represent the surfaces implicitly as the (zero) level-set of higher dimensional functions, and then efficiently solve the corresponding PDEs in the Cartesian coordinate system which contains the domain of this new embedding function.

The implicit representation of surfaces, here introduced for solving variational problems and PDEs, is inspired in part by the level-set work of Osher and Sethian [58]. This work, and those that followed it, showed the importance of representing deforming surfaces as level-sets of functions with higher dimensional domains, obtaining more robust and accurate numerical algorithms (and topological freedom). Note that, in contrast with the level-set approach of Osher and Sethian, both our domain and target manifold are fixed, what is "deforming" is the dataset defined on or onto it.

Solving PDEs and variational problems with triangulated meshes involves the non-trivial discretization of the equations on general polygonal grids, as well as the difficult numerical computation of other quantities like projections onto the discretized surface (when computing gradients and Laplacians for example). Although the use of triangulated surfaces is also quite popular in the brain imaging community, there is still no consensus on how to compute simple differential characteristics such as tangents, normals, principal directions, and curvatures. On the other hand, it is commonly accepted that computing these objects for iso-surfaces (implicit representations) is simpler and more accurate and robust [39, 56, 62, 65]. This problem becomes even more significant when we not only have to compute these first and second order differential characteristics of the surface, but also have to use them to solve variational problems and PDEs for data defined on the surface. Very little work has been done on the formal analysis of finite difference schemes on non-Cartesian meshes.[1] The computational cost of working with implicit representations is not higher than with meshes, since all the work is performed in a narrow band around the level-set(s) of interest.

Our framework of implicit representations enables us to perform all the computations on the Cartesian grid corresponding to the embedding function. These computations are, nevertheless, intrinsic to the surface. Advantages of using Cartesian grid instead of a triangulated mesh include the availability of well studied numerical techniques with accurate error measures and the topological flexibility of the surface, all leading to simple, accurate, robust and elegant implementations. If the surface is parameterized instead, or flattened to induce a mapping of planar coordinates onto it [37, 35], operations performed on the surface may depend on the particular triangulation and flattening of the surface, which is clearly problematic and not intrinsic. By contrast, the implicit approach is general (applicable to PDEs and variational problems beyond those derived in this paper), intrinsic/geometric, and dimensionality independent as well. Unless the framework proposed here is used, problems such as 3D warping of surfaces and shapes via PDEs has not be addressed without intermediate projections.

Numerical schemes that solve gradient descent flows and PDEs in and onto generic target manifolds will, in general, move the points outside of the target manifold $\mathcal{N}$, due to numerical errors. The points will then need to be projected back,[2] see for example [1, 16] for the case of $\mathcal{N}$ being a sphere (where the projection is trivial, just a normalization). For general target manifolds, this projection means that for every point $p \in I\!R^d$ ($\mathcal{N} \subset I\!R^d$) we need to know the closest point to p in $\mathcal{N}$. This means knowing the distance from every point $p \in I\!R^d$ to $\mathcal{N}$ (or at least all points in a band of $\mathcal{N}$). This is nothing other than an implicit representation of the target $\mathcal{N}$, being the particular embedding a distance function. This presents additional background for the framework introduced here, that is, if the embedding function for the surface has to

[1] Very important work has been done for finite element approaches, e.g., by the group of Prof. M. Rumpf, and on discretization of differential operators by M. Desbrun (see for example [20, 21]), as well as for particular equations on particular sub-division representations [5].

[2] For particular flat target manifolds as the whole space $I\!R^d$ or as those in [59], the projection is not needed. Other authors, e.g., [10, 41], have avoided the projection step for particular cases, while in [74] the authors extend [67] and modify the given variational formulation, in some restricted cases, to include the projection step.

be computed anyway for the projection, why not use it from the beginning if it helps in other steps of the computation?

The motivations to use implicit representations are not limited to computational considerations such as the one described above (including, as mentioned, the possibility to do 3D shape warping for the first time without intermediate projections). In the particular case of brain imaging, many of the state-of-the-art segmentation techniques reported in the literature are based on implicit representations [9, 29, 30, 39, 42, 32, 47, 56, 57, 62, 65, 83].[3] Therefore, it is not only computationally efficient but also completely natural to work within this framework, leaving the triangulation to the last step, meaning visualization, if at all needed. The framework described here can also be used for brain surfaces that are already extracted as mesh representations; they can first be turned into implicit form using the techniques reported in [23, 28, 44, 73], for example.

The remainder of this paper is organized as follows. In Section 2 we follow [48] and show how to compute geodesics on implicit surfaces. This leads to the ability to compute intrinsic distances as well as special curves such as sulcal fundi in the cortex. In Section 3 we follow [8] and show how to denoise maps defined on implicit surfaces. Based on [50], in Section 4 we show how to regularize surface warps, a technique that can be used for example to improve warps obtained following the techniques in [70], and extend the work in Section 2 to find curves constrained by landmarks. This section also discusses the application of brain and surface-to-surface warping in general. Section 5 concludes the paper.

2 Geodesic computations on implicit surfaces

Computing distance functions and geodesics on surfaces has a number of applications in brain imaging. For example, it can be used for finding cortical features such as sulci, for cortical surface flattening, for visualization, and for brain warping [38, 71, 76, 77], for correctly estimating spatial correlations in cortical fMRI signals [79], and for estimating the variability and distance between functional loci in the cortex.

Following [48], to which the reader is referred for details, an algorithm for the computationally optimal construction of intrinsic weighted distance functions on implicit hyper-surfaces is described in this section. The basic idea is to approximate the intrinsic weighted distance by the Euclidean weighted distance computed in a band surrounding the implicit hyper-surface in the embedding space, thereby performing all the computations in a Cartesian grid with classical and efficient numerics. Based on work on geodesics on Riemannian manifolds with boundaries, we bounded the error between the two distance functions. We showed that this error is of the same order as the theoretical numerical error in computationally optimal, Hamilton-Jacobi based, algorithms for computing distance functions in Cartesian grids. Therefore, we can use these algorithms, modified to deal with spaces with boundaries, and also obtain a computationally efficient technique for computing intrinsic distance functions on implicit hyper-surfaces.

Let us formally define the concept of *intrinsic* weighted distances on *implicit* hyper-surfaces. Let $\mathcal{S}$ be a (codimension 1) hyper-surface in $\mathbb{R}^d$ defined as the zero level set of a function $\psi : \mathbb{R}^d \to \mathbb{R}$. That is, $\mathcal{S}$ is given by $\{x \in \mathbb{R}^d : \psi(x) = 0\}$. We assume from now on that ψ is a signed distance function to the surface $\mathcal{S}$. Our goal is, for a given point $p \in \mathcal{S}$, to compute the intrinsic g-weighted distance function $d^g_{\mathcal{S}}(p, x)$ for all desired points $x \in \mathcal{S}$. We are referring to the intrinsic g-distance, that is, the geodesic distance on the Riemannian manifold $(\mathcal{S}, g^2\mathbf{I})$ ($\mathbf{I}$ stands for the $(d-1) \times (d-1)$ identity matrix) and not on the embedding Euclidean space. For a given positive weight g defined on the surface (we are considering only isotropic metrics for now), the g-distance on $\mathcal{S}$ (that coincides with the geodesic distance of the Riemannian manifold

[3] In particular, see the ITK initiative, which has implemented many of these techniques (www.itk.org).

$(\mathcal{S}, g^2\mathbf{I})$) is given by

$$d^g_{\mathcal{S}}(p,x) \stackrel{\triangle}{=} \inf_{\mathcal{C}_{px}[\mathcal{S}]} \{\mathbf{L}_g(\mathcal{C})\},$$

where

$$\mathbf{L}_g\{\mathcal{C}\} \stackrel{\triangle}{=} \int_a^b g\left(\mathcal{C}(l)\right) \, \|\dot{\mathcal{C}}(l)\| \, dl,$$

is the weighted *length functional* defined for piecewise C^1 curves $\mathcal{C} : [a,b] \to \mathcal{S}$, and $C_{px}[\mathcal{S}]$ denotes the set of curves that are piecewise C^1 joining p to x, traveling on $\mathcal{S}$. In general we will consider the definition to be valid for any $\tilde{g}$ defined over the domain that the curve may travel through.

We need to compute this distance when all the relevant objects are computationally represented in discrete form in the computer. Computing minimal weighted distances and paths in graph representations is an old problem that has been optimally solved by Dijkstra [22]. Dijkstra showed an algorithm for computing the path in $O(n \log n)$ operations, where n is the number of nodes in the graph. The weights are given on the edges that connect between the graph nodes, and the algorithm is computationally optimal. In theory, we could use this algorithm to compute the weighted distance and corresponding path on polygonal (not implicit) surfaces, with the vertices as the graph nodes and the edges the connections between them (see [43]). The problem is that the optimal paths computed by this algorithm are limited to travel on the graph edges, giving only a first approximation of the true distance. Moreover, Dijkstra's algorithm is not a consistent one: it will not converge to the true desired distance when the graph and grid are refined [54, 55]. The solution to this problem, limited to Cartesian grids, was developed in [33, 63, 64, 72]. Tsitsiklis first described an optimal-control type of approach, while independently Sethian and Helmsen both developed techniques based on upwind numerical schemes. The solution presented by these authors is consistent and converges to the true distance [61, 72], while keeping the same optimal complexity of $O(n \log n)$. This work was later extended in [40] for triangulated surfaces (see also [7, 45] for related works on numerics on non-Cartesian grids). We should note that the algorithm developed in [40] is currently developed only for triangulated surfaces with acute triangles. Therefore, before the algorithm can be applied, as an initialization step the surfaces have to be pre-processed to remove all obtuse triangles or other polygons present in the representation [39]. Following [64], we call these *fast marching algorithms*.

The basic idea behind the computationally optimal techniques for finding weighted distances, fast marching algorithms, is to note that the distance function satisfies a Hamilton-Jacobi Partial Differential Equation (PDE) in the viscosity sense (a theory for PDEs with singular solutions, [18]), given by

$$\|\nabla_{\mathcal{S}} d^g_{\mathcal{S}}\| = g \tag{1}$$

where $\nabla_{\mathcal{S}}$ is the gradient intrinsic to the surface, and $d^g_{\mathcal{S}}$ is the g-distance from a given seed point to the rest of the manifold.[4]

We transformed the problem of optimal distance computation into the problem of solving a Hamilton-Jacobi equation (recall that g is known, it is the given weight), also known as the Eikonal equation. In order to solve this equation, the current state of knowledge permits us to accurately and optimally (in a computational sense) find (weighted) distances on Cartesian grids as well as on particular triangulated surfaces (after some pre-processing, namely the elimination of obtuse triangles, see [6, 40]). The equation can also be solved in a (computationally non-efficient) evolution fashion [11]. We will describe how to solve the above Eikonal equation for implicit hyper-surfaces $\mathcal{S}$.

[4] $\nabla_{\mathcal{S}}$ and $d^g_{\mathcal{S}}$ become the classical gradient and distance respectively for Euclidean spaces.

The basic idea presented in [48] is conceptually very simple. We first consider a small h offset of $\mathcal{S}$. That is, since the embedding function ψ is a distance function, with $\mathcal{S}$ as its zero level set, we consider all points x in $\mathbb{R}^3$ for which $|\psi(x)| \leq h$. This gives a region in $\mathbb{R}^d$ with boundaries. We then modify the (Cartesian) fast marching algorithm mentioned above for computing the distance transform inside this h-band surrounding $\mathcal{S}$. Note that here, all the computations are performed as in [33, 63, 64, 72], in a Cartesian grid. We then use this Euclidean distance function as an approximation of the intrinsic distance on $\mathcal{S}$. In [48, 49] we have shown that this not only produces computationally optimal techniques (following the optimality of the fast marching algorithm), but also the error introduced by this approximation is of the same order or lower than the best error that can be obtained from the numerical approximation. We therefore lose nothing by using this technique, and gain the ability to use well-developed Cartesian algorithms. An example is given in Figure 1, where the geodesic is obtained as an intrinsic gradient descent in the direction of the computed intrinsic distance $d^g_{\mathcal{S}}$.

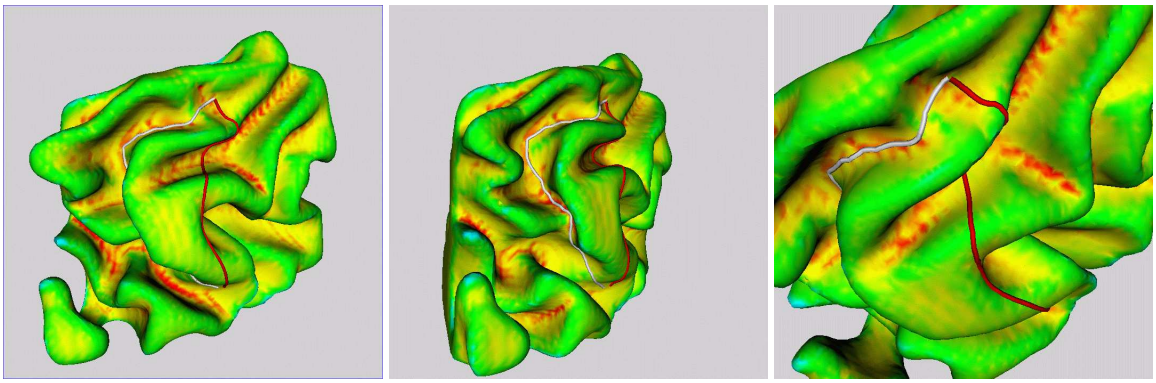

Figure 1: Detection of sulcal fundi over implicit surfaces representing a portion of the human cortex. We use a mean curvature based weighted distance (as in [7]). We show two curves over the surface, whose coloring correspond to the mean curvature (not clipped, from red, yellow, green to blue, as the value increases). The red curve is the one that corresponds to the *natural* geodesic ($g = 1$), while the white curve is the weighted-geodesic that should travel through "nether" regions, such as sulcal beds. Indeed, a very clear difference exists between both trajectories, since the white curve makes its way through regions where the mean curvature attains low values. The figure on the right is a zoomed view of the same situation. *(This is a color figure.)*

3 Regularizing maps on the cortical surface

In this section we show how to use the framework developed in [8] for regularizing data on the cortical surface. In particular, as an application, we regularize a scalar field representing the gray matter thickness, but other (scalar and beyond) fields such as fMRI or EEG signals can be regularized with this technique as well (see [24] and paper by Faugeras *et al.* in this issue). To make the presentation easier, we discuss the regularization via the Laplace-Beltrami flow (see also [13, 14, 15]), while of course other PDEs or variational formulations could be used as well.

We assume as before that the two dimensional surface $\mathcal{S}$ of interest (here the cortex) is given in implicit form, as the zero level set of a given function $\psi : \mathbb{R}^3 \rightarrow \mathbb{R}$, with $\mathcal{S} \equiv \{x \in \mathbb{R}^3 : \psi(x) = 0\}$. To ensure that the data, which does not need to be defined outside of the surface originally, is now defined in the whole band, one simple possibility is to extend this data u defined on $\mathcal{S}$ (i.e the zero level set of ψ) in such a form that it is constant normal to each level set of ψ, see [8] for details.

We illustrate the framework in [8] with the simplest case, the heat flow or Laplace equation for scalar data defined on a surface. For scalar data u defined on the plane, that is, $u(x,y) : I\!R^2 \to I\!R$ it is well known that the heat flow $\frac{\partial u}{\partial t} = \Delta u$, where $\Delta := \frac{\partial^2 u}{\partial x^2} + \frac{\partial^2 u}{\partial y^2}$ is the Laplacian, is the gradient descent flow of the Dirichlet integral $\frac{1}{2}\int_{I\!R^2} \parallel \nabla u \parallel^2 dxdy$, where ∇ is the gradient. This flow performs smoothing of the scalar data u, and this smoothing process progressively decreases the abovementioned energy. If we now want to smooth scalar data u defined on a surface $\mathcal{S}$, we must consider the gradient descent of the *harmonic* energy given by

$$\frac{1}{2}\int_{\mathcal{S}} \parallel \nabla_{\mathcal{S}} u \parallel^2 d\mathcal{S}, \tag{2}$$

The gradient descent flow for this energy is

$$\frac{\partial u}{\partial t} = \Delta_{\mathcal{S}} u. \tag{3}$$

Here $\nabla_{\mathcal{S}}$ is the intrinsic gradient and $\Delta_{\mathcal{S}}$ the intrinsic Laplacian or Laplace-Beltrami operator. These are classical concepts in differential geometry, and are basically the natural extensions of the gradient and Laplacian respectively, considering all derivatives intrinsic to the surface (with the natural metric). For instance, as noted below, the intrinsic gradient is just the projection onto the tangent space to $\mathcal{S}$ of the usual $3D$ gradient while the Laplace-Beltrami operator is the projected divergence of it [66].

Using the implicit framework, we proceed now to redefine the above energy and compute its corresponding gradient descent flow. Let $\vec{v}$ be a generic three dimensional vector, and $P_{\vec{v}}$ the operator that projects a given three dimensional vector onto the plane orthogonal to $\vec{v}$: $P_{\vec{v}} := \mathbf{I} - \frac{\vec{v}\otimes\vec{v}}{\|\vec{v}\|^2}$. It is then easy to show that the harmonic energy (2) is equivalent to (see for example [66])

$$\frac{1}{2}\int_{\mathcal{S}} \parallel P_{\vec{N}} \nabla u \parallel^2 d\mathcal{S}, \tag{4}$$

where $\vec{N}$ is the normal to the surface $\mathcal{S}$. In other words, $\nabla_{\mathcal{S}} u = P_{\vec{N}} \nabla u$. That is, the gradient intrinsic to the surface ($\nabla_{\mathcal{S}}$) is just the projection onto the surface of the 3D Cartesian (classical) gradient ∇. We now embed this in the function ψ:

$$\frac{1}{2}\int_{\mathcal{S}} \parallel \nabla_{\mathcal{S}} u \parallel^2 d\mathcal{S} = \frac{1}{2}\int_{\mathcal{S}} \parallel P_{\vec{N}} \nabla u \parallel^2 d\mathcal{S} = \frac{1}{2}\int_{\Omega\in I\!R^3} \parallel P_{\nabla\psi} \nabla u \parallel^2 \delta(\psi) \parallel \nabla\psi \parallel dx,$$

where $\delta(\cdot)$ stands for the delta of Dirac, and all the expressions above are considered in the sense of distributions. Note that first we got rid of intrinsic derivatives by replacing $\nabla_{\mathcal{S}}$ by $P_{\vec{N}}\nabla u$ (or $P_{\nabla\psi}\nabla u$) and then replaced the intrinsic integration ($\int_{\mathcal{S}} d\mathcal{S}$) by the explicit one ($\int_{\Omega\in I\!R^3} dx$) using the delta function. Intuitively, although the energy lives in the full space, the delta function forces the penalty to be effective only on the level set of interest. The last equality includes the embedding, and it is based on the fact that $\nabla\psi \parallel \vec{N}$ and $\int_\Omega \delta(\psi) \parallel \nabla\psi \parallel dx = \int_{\mathcal{S}} d\mathcal{S} =$ surface area. The gradient descent of this energy is given by [8]

$$\frac{\partial u}{\partial t} = \nabla \cdot (P_{\nabla\psi} \nabla u). \tag{5}$$

In other words, this equation corresponds to the intrinsic heat flow or Laplace-Beltrami flow for data defined on an implicit surface. But all the gradients in this PDE are defined in the three dimensional Cartesian space, not in the surface $\mathcal{S}$ (this is why we need the data to be defined at least on a band around the surface). The numerical implementation is then straightforward. This is the beauty of the approach! Basically, for this

equation we use a classical scheme of forward differences in time and a succession of forward and backward differences in space. See [8] for details as well as equations for other variational measures and PDEs.

As an example, we apply this framework to the regularization of thickness maps. To quantify cortical gray matter thickness, see Figure 2, we use the 3D distance measured from the cortical white-gray matter boundary in the tissue classified brain volumes to the cortical surface (gray-CSF boundary) in each subject. Tissue classified brain volumes were resampled into .33 mm cubic voxels (as in Miller *et al.* [52]) to obtain distance measures indexing gray matter thickness at sub-voxel spatial resolution. Gray matter thickness was then measured at thousands of homologous cortical locations in each subject. Gray matter thickness measures may again be averaged and compared at each cortical surface location providing spatially detailed maps of local thickness differences within or between groups. This is of course just one way of measuring thickness, and is used here to illustrate the computational framework. Other methods could be used as well, such as those developed by Jones *et al.* [36], Yezzi and Prince [81], Annese *et al.* [2], Fischl *et al.* [25], Lerch *et al.* [46], and Miller *et al.*, [52].

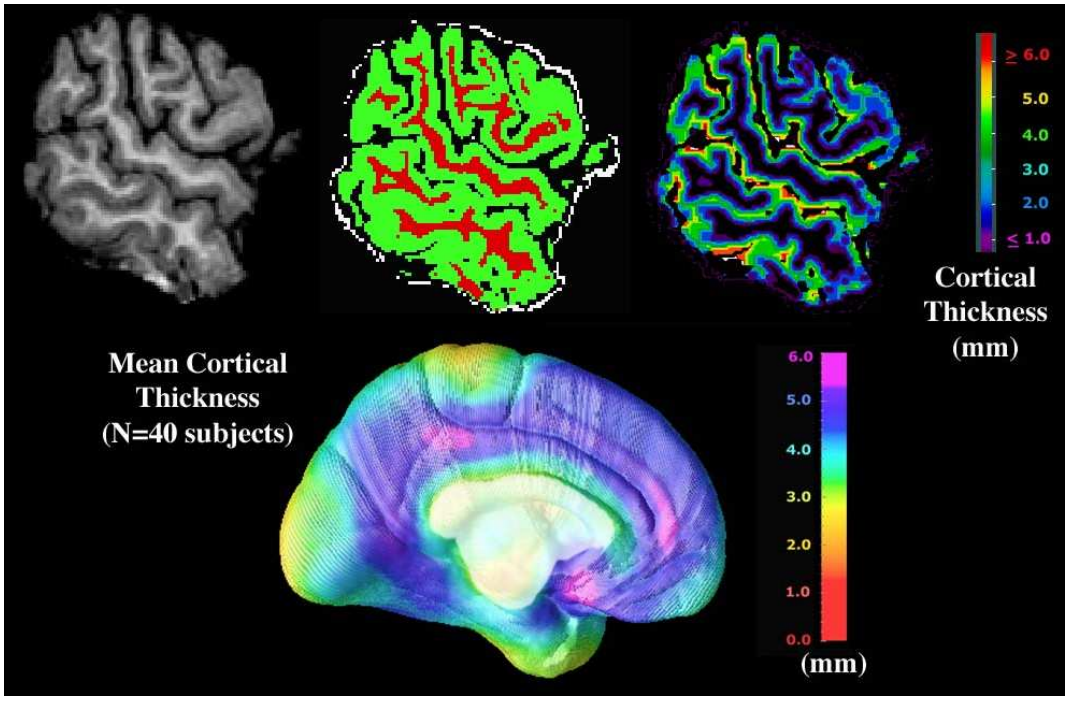

Figure 2: Illustration of cortical thickness maps. The top row (left panel) shows a sagittal section through a T1-weighted brain MRI scan, and a classification (middle panel) of the image into gray matter (green colors) and white matter (red colors), as well as extracerebral tissue and background (white and black colors). The top right panel shows the cortical thickness estimated as the distance from the gray-white interface to each gray matter voxel in the cortex. The lower panel shows the spatial profile of mean cortical thickness in a set of 40 healthy young adults; the cortex is thinnest in primary visual and sensorimotor regions, and thickest in the posterior cingulate and paralimbic cortices. Here averaging of thickness values was performed after matching homologous cortical regions using cortical sulci as constraints [70]. Cortical thickness is not defined in the corpus callosum and ventricular regions (here masked out in white). *(This is a color figure.)*

In Figure 3 we apply the formulation above (Laplace-Beltrami flow for data on an implicitly represented brain), to regularize a scalar field that represents an estimate of the gray matter thickness on the cortex. We present the results for 0 (initial condition), 25, 50, and 100 iterations, from left to right respectively.

Two views are shown in the figure, one in each row. We should mention that the brain model used for this exercise is coarse, and that the total energy (integral of thickness measure over the whole surface) has been numerically preserved.

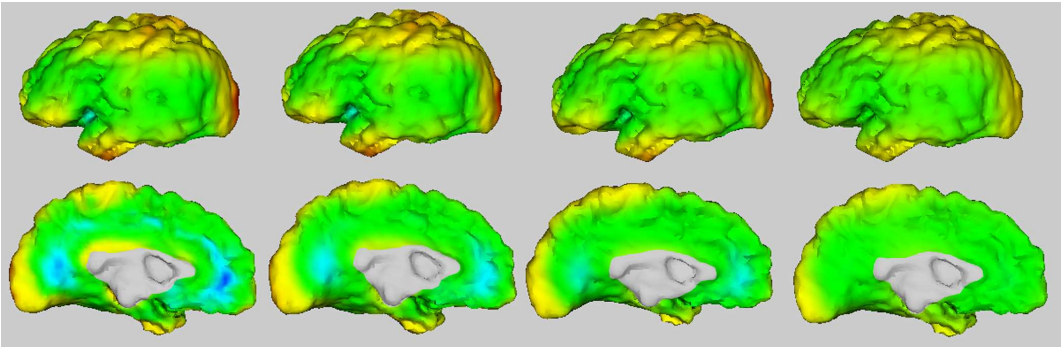

Figure 3: Regularizing cortical thickness maps. Two views are presented (top row: lateral surface; bottom row: medial surface), each showing 0 (initial condition), 25, 50, and 100 steps (from left to right respectively) of the Laplace-Beltrami flow for data on an implicit surface representing a coarse model of the brain. *(This is a color figure.)*

4 Maps between implicit surfaces

Following the result of the previous section, the next step is to consider maps from a generic manifold $\mathcal{M}$ onto another generic one $\mathcal{N}$, which is not just restricted to the real line as in Section 3 or other simple manifolds as considered in [8, 59, 67]. For example, this generality is needed when solving brain warping problems via PDEs [71], such as cortical flattening [35], or nonlinear registration of 3D surfaces and volumes across subjects or across time (e.g., in mapping brain growth). Typically the nonlinear registration of one cortical surface to another is addressed in the literature via intermediate distorting projections onto the plane [35] or 3D sphere ([70, 78, 31]).

In [50], we have addressed this general problem, and this section will briefly describe the approach and present examples.

As before, we assume that the target manifold $\mathcal{N}$ is given as the zero level set of a higher dimensional embedding function $\psi : I\!R^d \rightarrow I\!R$, which we consider to be a signed distance function. For simplicity of the presentation, we assume that the domain manifold $\mathcal{M}$ is flat and open, since the general case of $\mathcal{M}$ was dealt with in Section 3. We also illustrate the basic ideas with a functional from the theory of harmonic maps, while others will be used for the examples below. The harmonic map is not the ideal one for applications of brain warping, since higher order functionals are needed (and also it is necessary to deal with the hard landmark constraints, such as the enforcement of sulcal correspondences when one brain is matched to another). From the presentation below, it will be clear how to extend the formulation to maps more relevant to brain imaging. We search for necessary conditions for the functional $E[\vec{u}]$, defined by

$$E[\vec{u}] \stackrel{\triangle}{=} \int_{\mathcal{M}} e[\vec{u}]\, d_{\mathcal{M}} v \tag{6}$$

where $e[\vec{u}] \stackrel{\triangle}{=} \frac{1}{2}\|\mathbf{J}_{\vec{u}}\|^2_{\mathcal{F}}$, to achieve a minimum. Here, $\|\cdot\|^2_{\mathcal{F}} = \sum_{ij}(\cdot)^2_{ij}$ is the norm of Frobenius and $\mathbf{J}_{\vec{u}}$ is the Jacobian of the map $\vec{u} : \mathcal{M} \rightarrow \{\psi = 0\}$. We are already restricting the map to be onto the zero level-set of ψ, that is, onto the surface of interest $\mathcal{N}$ (the target manifold). This is what permits us to work with the

embedding function and the whole space, while guaranteeing that the map will always be onto the target manifold, as desired.[5]

Proposition 1 ([50]) *The Euler-Lagrange of Equation (6), is given by*

$$\Delta\vec{u} + \left(\sum_k \mathbf{H}_\psi \left[\frac{\partial\vec{u}}{\partial x_k}, \frac{\partial\vec{u}}{\partial x_k}\right]\right) \nabla\psi(\vec{u}) = 0, \tag{7}$$

where $\mathbf{H}_\psi$ stands for the Hessian of the embedding function ψ (and we used the notation $A[\vec{x}, \vec{y}] = \vec{y}^T A\,\vec{x}$). The solution to this equation is a map onto the zero level-set of ψ.

This equation then gives the corresponding Euler-Lagrange for the given variational problem (and from it we get the gradient-descent flow, with Neumann boundary conditions). Note once again from our computations, that despite the fact that all the terms "live" in the Euclidean space where the target manifold is embedded, $\vec{u}$ will always map onto the level-set of interest, $\{\psi = 0\}$, and therefore, onto the surface of interest. This is guaranteed by this equation, no additional computations are needed. As before, this is the beauty of the approach, while working freely on the Euclidean space (and therefore with Cartesian numerics), we can guarantee that the equations are intrinsic to the given surfaces of interest. Additional theory and examples are provided in [50], including the complete equations when this framework is combined with the one described in Section 3, as well as the theory for open target manifolds.

We now present two examples of the above formulation for solving maps between two implicit surfaces using Cartesian numerics. First, $\mathcal{M}$ is a segment of $\mathbb{R}^1$ and $\mathcal{N}$ a 3D implicit cortex. Then, $\vec{u}$ is a curve on the cortex, and our goal is to compute a smooth curve that passes through a number of previously marked points (landmarks). Without the constraints given by the points, the solution will be a geodesic. The curve is forced to go through the points (or close to them) simply by adding a term that penalizes its distance to the landmarks.[6] The resulting gradient descent flow is solved with implicit numerics. Figure 4, first row, presents a first example, where we clearly see the evolution of the yellow curve to the constrained black one. On the second and third rows we extend this for the computation of the sulcal bed, constrained by a few given points (regular view on the left and zoomed in one on the right). For this, we add a third term that penalizes paths that move away from the sulcal bed [6, 48].

The next example deals with the case when both $\mathcal{M}$ and $\mathcal{N}$ are surfaces. Figure 5 shows a map from an implicit torus to an implicit bunny using the harmonic mapping energy. This example shows the applicability of our framework to the problem of constructing mappings between manifolds. In the example, an initial map from the torus to the bunny is constructed and then a simply-connected region (blue colors) is defined on the bunny, this blue region corresponds to the image of the whole torus through this initial map. The subsequent diffusion of this initial map is shown in this way, that is, changes in the map can be seen through changes in the blue region. Diffusions and flows can then be defined on the second manifold without any need to parameterize either of the surfaces, or flatten them. For brain image warping, this idea could be used to warp one 3D brain surface directly onto another, enforcing constraints such as the matching of sulcal curves lying in the surface [70], or regions with corresponding surface curvature [25]. Normally, this is done by parameterizing each surface, and defining a matching energy between features on each surface. If the surface is parameterized, great caution is required to ensure that the matching fields between surfaces do not depend on the specific details of how the surfaces are parameterized (see e.g. [70], for an approach

[5] We use $\vec{\cdot}$ to note that for the most general case, the function is vectorial.

[6] In contrast with [34], the energy is intrinsic to the manifold and there is no parametrization, meaning we do not enforce certain points on the curve to be attracted to a given landmark.

based on covariant PDEs, where the Christoffel symbols of the surface metric are used). With an implicit approach, the need to parameterize each surface is completely avoided. This results in simpler and more accurate numerical implementations. For matching of two brain surfaces in implicit form, the idea is to start from an approximate initial map between these two surfaces and regularize it using our implicit framework and a suitably defined functional. This could be a compound functional including the harmonic energy, as above, and a data fidelity term that could include landmark or curvature-based constraints when mapping one surface to another. These surface-based mappings are required for making average maps of cortical features across subjects, such as the mean cortical thickness map shown in Figure 2. We are currently working on using energies on implicit functions to define the warping map between two general curved manifolds, without of course any intermediate projection to the plane or sphere as is typically done in the literature, see [51].

5 Discussion

In this paper we have shown how implicit surface representations, as obtained from the state-of-the-art brain segmentation algorithms, are useful for addressing a number of the fundamental problems in brain imaging. The key idea is that once the surfaces are represented in implicit form, solving variational problems and PDEs between them is as straightforward as working with flat domains, and Cartesian numerics can be used. This avoids common parametrization and flattening techniques, which are either non-intrinsic and/or introduce errors into the solution. In the future we plan to extend the examples presented here and apply them to population studies of brain structure and function.

Acknowledgments

This work is partially supported by ONR, NSF, NIH, and CSIC-Uruguay. Additional support was provided by the National Institute of Biomedical Imaging and Bioengineering (grant R21 EB01561) and National Center for Research Resources (R21 RR019771). We thank Prof. Stanley Osher for ongoing collaboration on solving PDEs on and onto manifolds.

References

[1] F. Alouges, "An energy decreasing algorithm for harmonic maps," in J.M. Coron *et al.*, Editors, *Nematics*, Nato ASI Series, Kluwer Academic Publishers, Netherlands, pp. 1-13, 1991.

[2] J. Annese, A. Pitiot, I.D. Dinov, A.W. Toga,"A myelo-architectonic method for the structural classification of cortical areas," *Neuroimage*, **21(1)**, pp. 15-26, 2004.

[3] S. Angenent, S. Haker, A. Tannenbaum, and R. Kikinis, "Conformal geometry and brain flattening," *Proc. MICCAI*, pp. 271-278, 1999.

[4] J. Ashburner and K. J. Friston, "Nonlinear spatial normalization using basis functions," *Hum. Brain Mapp.* **7(4)**, pp. 254-66, 1999.

[5] C. Bajaj, G. Xu, "Anisotropic diffusion of subdivision surfaces and functions on surfaces," *ACM Transactions on Graphics* **22:1**, pp. 4-32, 2003.

[6] A. Bartesaghi and G. Sapiro, "A system for the generation of curves on 3D brain images," *Human Brain Mapping* **14:1**, pp. 1-15, 2001.

[7] T. J. Barth and J. A. Sethian, "Numerical schemes for the Hamilton-Jacobi and level set equations on triangulated domains," *Journal of Computational Physics* **145**, pp. 1-40, 1998.

[8] M. Bertalmio, L. T. Cheng, S. Osher, and G. Sapiro, "Variational problems and partial differential equations on implicit surfaces," *Journal of Computational Physics,* **174:2**, pp. 759-780, 2001.

[9] V. Caselles, R. Kimmel, G. Sapiro, and C. Sbert, "Minimal surfaces based object segmentation," *IEEE-PAMI*, **19:4**, pp. 394-398, April 1997.

[10] T. Chan and J. Shen, " Restoration of non-flat image features: models and algorithms", *SIAM J. Appl. Math.*, **61(4)**, pp. 1338-1361, 2000.

[11] L. T. Cheng, "The level set method applied to geometrically based motion, materials science, and image processing (Ph.D. Thesis)," *CAM-UCLA Report* **00-20**, June 2000

[12] G. E. Christensen, R. D. Rabbitt, and M. I. Miller, "A deformable neuroanatomy textbook based on viscous fluid mechanics." Invited paper. In Prince and Runolfsson, editors, *Proceedings of the 1993 Conference on Information Sciences and Systems*, Johns Hopkins University, March 24-26, 1993, pp. 211-216.

[13] M. K. Chung, K. J. Wosley, J. Taylor, J. Ramsay, S. Robbins, and A. C. Evans, "Diffusion smoothing on the cortical surface," *Neuroimage* **13S**, pp. 95, 2001.

[14] M.K. Chung, K.J. Worsley, S. Robbins, T. Paus, J. Taylor, J.N. Giedd, J.L. Rapoport and A.C. Evans, "Deformation-based surface morphometry applied to gray matter deformation," *Neuroimage*, **18(2)**, pp. 198-213, 2003.

[15] M.K. Chung and J. Taylor, "Diffusion Smoothing on Brain Surface via Finite Element Method,"*IEEE International Symposium on Biomedical Imaging*, poster 562, 2004.

[16] R. Cohen, R. M. Hardt, D. Kinderlehrer, S. Y. Lin, and M. Luskin, "Minimum energy configurations for liquid crystals: Computational results," in J. L. Ericksen and D. Kinderlehrer, Editors, *Theory and Applications of Liquid Crystals*, pp. 99-121, IMA Volumes in Mathematics and its Applications, Springer-Verlag, New York, 1987.

[17] D. L. Collins, T. M. Peters, and A. C. Evans, "An automated 3D non-linear image deformation procedure for determination of gross morphometric variability in the human brain," *Proc. Visualization in Biomed. Comp. (SPIE)* **3**, pp. 180-190, 1994.

[18] M. G. Crandall, H. Ishii, and P. L. Lions, "User's guide to viscosity solutions of second order partial linear differential equations," *Bulletin of the American Math. Society* **27**, pp. 1-67, 1992.

[19] C. Davatzikos, "Spatial normalization of 3D brain images using deformable models," *J. Comp. Assisted Tomography* **20(4)**, pp. 656-665, 1996.

[20] M.P. Cani-Gascuel and M.Desbrun, "Animation of Deformable Models using Implicit Surfaces," *IEEE Transactions on Vision and Computer Graphics*, **3(1)**, pp. 39-50, 1997.

[21] M. Desbrun and M.P. Cani-Gascuel, "Active Implicit Surface for Animation," *Graphics Interface'98*, pp. 143-150, 1998.

[22] E. Dijkstra, "A note on two problems in connection with graphs," *Numerische Math.* **1**, pp. 269-271, 1959.

[23] M. Eck and H. Hoppe, "Automatic reconstruction of B-spline surfaces of arbitrary topological type," *Proceedings of the 23rd annual conference on Computer graphics and interactive techniques*, pp. 325-334, 1996.

[24] O. Faugeras, F. Clément, R. Deriche, R. Keriven, T. Papadopoulo, J. Gomes, G. Hermosillo, P. Kornprobst, D. Lingrad, J. Roberts, T. Viéville, F. Devernay, "The inverse EEG and MEG problems: The adjoint state approach I: The continuous case," *INRIA Research Report* **3673**, June 1999.

[25] B. Fischl, M. I. Sereno, R. B. H. Tootell, and A. M. Dale, "High-resolution inter-subject averaging and a coordinate system for the cortical surface," *Hum Brain Mapp.* **8(4)**, pp. 272-84, 1999.

[26] P. A. Freeborough and N. C. Fox, "Modeling brain deformations in Alzheimer's disease by fluid registration of serial 3D MR images," *J Comput Assist Tomogr* **22**, pp. 838-43, 1998.

[27] N. C. Fox, W. R. Crum, R. I. Scahill, J. M. Stevens, J. C. Janssen, and M. N. Rossor, "Imaging of onset and progression of Alzheimer's disease with voxel-compression mapping of serial magnetic resonance images," *Lancet* **358**, pp. 201-205, 2001.

[28] S. F. Frisken, R. N. Perry, A. Rockwood, and T. Jones, "Adaptively Sampled Distance Fields: A General Representation of Shape for Computer Graphics," *Proc. SIGGRAPH 2000*, pp. 249-254, 2000.

[29] J. Gomes and O. Faugeras, "Reconciling distance functions and level sets," *Proc. Scale Space Theory in Computer Vision*, pp. 70-81, LNCS 1682, Berlin, 1999.

[30] R. Goldenberg, R. Kimmel, E. Rivlin and M. Rudzsky, "Cortex Segmentation - A fast variational geometric approach," *IEEE Trans. on Medical Imaging,* **21(2)**, pp. 1544-1551, Dec. 2002.

[31] X. Gu, Y.L. Wang, T.F. Chan, P.M. Thompson and S.T. Yau, "Genus Zero Surface Conformal Mapping and its Application to Brain Surface Mapping," *IEEE Transactions on Medical Imaging*, **23(7)**, 2004.

[32] X. Han, C. Xu and J.L. Prince, " A topology preserving geometric deformable model and its application in brain cortical Surface Reconstruction," in S. Osher and N. Paragios eds, *Geometric Level Set Methods in Imaging, Vision and Graphics*, Springer Verlag, 2003.

[33] J. Helmsen, E. G. Puckett, P. Collela, and M. Dorr, "Two new methods for simulating photolithography development in 3D," *Proc. SPIE Microlithography* **IX**, pp. 253, 1996.

[34] M. Hofer and H. Pottmann, "Energy-minimizing splines in manifolds," *ACM Trans. on Graphics (SIGGRAPH '04)*, July 2004.

[35] M. K. Hurdal, P. L. Bowers, K. Stephenson, D. W. L. Sumners, K. Rehm, K. Schaper and D. A. Rottenberg, "Quasi-conformally flat mapping the human cerebellum," in C. Taylor and A. Colchester (eds), *Medical Image Computing and Computer-Assisted Intervention - MICCAI'99*, Vol. 1679 of Lecture Notes in Computer Science, Springer, Berlin, pp. 279-286, 1999.

[36] S.E. Jones, B.R. Buchbinder and I. Aharon, "Three-dimensional mapping of cortical thickness using Laplace's equation," *Hum Brain Mapp.*, **11(1)**, pp. 12-32, 2000.

[37] L. Ju, J. Stern, K. Rehm, K. Schaper, M. Hurdal and D. Rottenberg, "Cortical Surface Flattening using Least Square Conformal Mapping with Minimal Metric Distortion," *Proceedings of the Second IEEE International Symposium on Biomedical Imaging*, pp. 77-80, 2004.

[38] N. Khaneja, M.I. Miller, and U. Grenander, "Dynamic programming generation of geodesics and sulci on brain surfaces," *IEEE Trans. on Pattern Analysis and Machine Intelligence* **20:11**, pp.1260-1265, November, 1998.

[39] R. Kimmel, *Numerical Geometry of Images: Theory, Algorithms, and Applications*, Springer-Verlag, New York, 2004.

[40] R. Kimmel and J. A. Sethian, "Computing geodesic paths on manifolds," *Proc. National Academy of Sciences* **95:15**, pp. 8431-8435, 1998.

[41] R. Kimmel and N. Sochen. "Orientation Diffusion or How to Comb a Porcupine?," *Journal of Visual Communication and Image Representation*, **13**, pp. 238-248, 2002.

[42] S. Kichenassamy, A. Kumar, P. Olver, A. Tannenbaum, and A. Yezzi, "Conformal curvature flows: from phase transitions to active vision," *Archive for Rational Mechanics and Analysis* **134**, pp. 275-301, 1996.

[43] N. Kiryati and G. Székely, "Estimating shortest paths and minimal distances on digitized three dimensional surfaces," *Pattern Recognition* **26**, pp. 1623–1637, 1993.

[44] V. Krishnamurthy and M. Levoy, "Fitting smooth surfaces to dense polygon meshes," *Computer Graphics*, pp. 313-324, 1996.

[45] F. Lafon and S. Osher, "High order two dimensional nonoscillatory methods for solving Hamilton-Jacobi scalar equations," *Journal of Computational Physics* **123**, pp. 235-253, 1996.

[46] J. Lerch, J. Pruessner, A. Zijdenbos and A. Evans, "A Population Simulation Validation Study of Cortical Thickness Analysis," Meeting of the Organization for Human Brain Mapping, 2003, Poster number 868, `http://208.164.121.55/hbm2003/abstract/abstract868.htm`.

[47] R. Malladi, J. A. Sethian and B. C. Vemuri, "Shape modeling with front propagation: A level set approach," *IEEE Trans. on PAMI* **17**, pp. 158-175, 1995.

[48] F. Mémoli and G. Sapiro, "Fast computation of weighted distance functions and geodesics on implicit hyper-surfaces," *Journal of Computational Physics,* **173:2**, pp. 730-764, November 2001.

[49] F. Mémoli and G. Sapiro, "Distance functions and geodesics on point clouds," *IEEE Workshop on Variational and Level-Sets Methods in Computer Vision*, Nice, France, October 2003.

[50] F. Mémoli, G. Sapiro, and S. Osher, "Solving variational problems and partial differential equations mapping into general target manifolds," *J. Comput. Phys.* **195**, pp. 263-292, March 2004.

[51] F. Mémoli, G. Sapiro, and P. Thompson, "Implicit brain warping," in preparation.

[52] M. I. Miller, M. Hosakere, A. R. Barker, C. E. Priebe, N. Lee, J. T. Ratnanather, L. Wang, M. Gado, J. C. Morris, and J. G. Csernansky "Labeled cortical mantle distance maps of the cingulate quantify differences between dementia of the Alzheimer type and healthy aging", *PNAS* **100**, pp. 15172-15177, 2003.

[53] M. I. Miller, A. Trouve, and L. Younes, "On the metrics and Euler-Lagrange equations of computational anatomy," *Ann. Rev. Biomed Eng.* **4**, pp. 375-405, 2002.

[54] J. S. B. Mitchell, "An algorithmic approach to some problems in terrain navigation," *Artificial Intelligence* **37**, pp. 171-201, 1988.

[55] J. S. B. Mitchell, D. Payton, and D. Keirsey, "Planning and reasoning for autonomous vehicle control," *International Journal of Intelligent Systems* **2**, pp. 129-198, 1987.

[56] S. J. Osher and R. Fedkiw, *Level Set Methods and Dynamic Implicit Surfaces*, Springer-Verlag, New York, 2003.

[57] S. J. Osher and N. Paragios, *Geometric Level Set Methods in Imaging, Vision, and Graphics,* Springer-Verlag, New York, 2003.

[58] S. J. Osher and J. A. Sethian, "Fronts propagation with curvature dependent speed: Algorithms based on Hamilton-Jacobi formulations," *Journal of Computational Physics* **79**, pp. 12-49, 1988.

[59] A. Pardo and G. Sapiro, "Vector probability diffusion," *IEEE Signal Processing Letters* **8**, pp. 106-109, April 2001.

[60] J.T. Ratnanather, P.E. Barta, N.A. Honeycutt, N. Lee, H.M. Morris, A.C. Dziorny, M.K. Hurdal, G.D. Pearlson and M.I. Miller, "Dynamic programming generation of boundaries of local coordinatized submanifolds in the neocortex: application to the planum temporale," *Neuroimage*, **20(1)**, pp. 359-377, 2003.

[61] E. Rouy and A. Tourin, "A viscosity solutions approach to shape-from-shading," *SIAM. J. Numer. Analy.* **29:3**, pp. 867-884, 1992.

[62] G. Sapiro, *Geometric Partial Differential Equations and Image Processing*, Cambridge University Press, January 2001.

[63] J. Sethian, "Fast marching level set methods for three-dimensional photolithography development," *Proc. SPIE International Symposium on Microlithography*, Santa Clara, California, March, 1996.

[64] J. A. Sethian, "A fast marching level-set method for monotonically advancing fronts," *Proc. Nat. Acad. Sci.* **93:4**, pp. 1591-1595, 1996.

[65] J. A. Sethian, *Level Set Methods: Evolving Interfaces in Geometry, Fluid Mechanics, Computer Vision and Materials Sciences,* Cambridge University Press, Cambridge-UK, 1996.

[66] L. Simon, *Lectures on Geometric Measure Theory*, Australian National University, Australia, 1984.

[67] B. Tang, G. Sapiro, and V. Caselles, "Diffusion of general data on non-flat manifolds via harmonic maps theory: The direction diffusion case," *Int. Journal Computer Vision* **36:2**, pp. 149-161, February 2000.

[68] P. Teo, G. Sapiro, and B. Wandell, "Creating connected representations of cortical gray matter for functional MRI visualization," *IEEE Trans. Medical Imaging* **16:06**, pp. 852–863, December 1997.

[69] P. M. Thompson, J. N. Giedd, R. P. Woods, D. MacDonald, A. C. Evans, and A. W. Toga, "Growth patterns in the developing brain detected by using continuum-mechanical tensor maps," *Nature* **404**, pp. 190-193., 2000.

[70] P. M. Thompson, R. P. Woods, M. S. Mega, and A. W. Toga, "Mathematical/computational challenges in creating population-based brain atlases," *Human Brain Mapping* **9(2)**, pp. 81-92, Feb. 2000.

[71] A. W. Toga, *Brain Warping*, Academic Press, New York, 1998.

[72] J. N. Tsitsiklis, "Efficient algorithms for globally optimal trajectories," *IEEE Transactions on Automatic Control* **40** pp. 1528-1538, 1995.

[73] G. Yngve and G. Turk, "Creating smooth implicit surfaces from polygonal meshes," *Technical Report GIT-GVU-99-42, Graphics, Visualization, and Usability Center. Georgia Institute of Technology*, 1999.

[74] L. A. Vese and S. J. Osher, "Numerical methods for p-harmonic flows and applications to image processing," *SIAM Journal on Numerical Analysis*, **40(6)**, pp. 2085-2104, 2002.

[75] D. C. Van Essen, H. Drury, S. Joshi and M. I. Miller, "Comparisons between human and macaque using shape-based deformation algorithms applied to cortical flat maps," *3rd Int. Conference on Functional Mapping of the Human Brain, NeuroImage* **5(4)**, Copenhagen, May 19-23, 1997.

[76] D. C. Van Essen, H. Drury, S. Joshi and M. I. Miller, "Functional and structural mapping of human cerebral cortex: Solutions are in the surfaces," *Proceedings of the National Academy of Science* **95**, pp. 788-795, February 1998.

[77] B. Wandell, S. Chial, and B. Backus, "Visualization and Measurement of the Cortical Surface." *Journal of Cognitive Neuroscience*, **12(5)**, pp. 739-752, 2000.

[78] Y.L Wang, X. Gu, T. Chan, P.M. Thompson and S.T. Yau, "Intrinsic Brain Surface Conformal Mapping using a Variational Method," *Proc. Medical Imaging Computing and Computer Assisted Intervention (MICCAI)*, Canada, November 2003.

[79] K. J. Worsley, M. Andermann, T. Koulis, D. MacDonald, and A. C. Evans, "Detecting changes in nonisotropic images," *Hum Brain Mapp.* **8(2-3)**, pp. 98-101., 1999.

[80] K. J. Worsley, S. Marrett, P. Neelin, and A. C. Evans, "Searching scale space for activation in PET images," *Human Brain Mapping* **4**, pp. 74-90, 1996.

[81] A. Yezzi and J. L. Prince, "An Eulerian PDE Approach for Computing Tissue Thickness," *IEEE Trans. Medical Imaging*, **22(10)**, pp. 1332-1339, 2003.

[82] M. M. Zeineh, S. A. Engel, P. M. Thompson, and S. Bookheimer, "Unfolding the human hippocampus with high-resolution structural and functional MRI," *The New Anatomist (Anatomical Record)* **265(2)**, pp. 111-120, 2001.

[83] X. Zeng, L. H. Staib, R. T. Schultz, and J. S. Duncan, "Segmentation and meassurements of the cortex from 3D MR images using coupled surfaces propagation," *IEEE Trans. Medical Imaging* **18**, pp. 927-937, 1999.

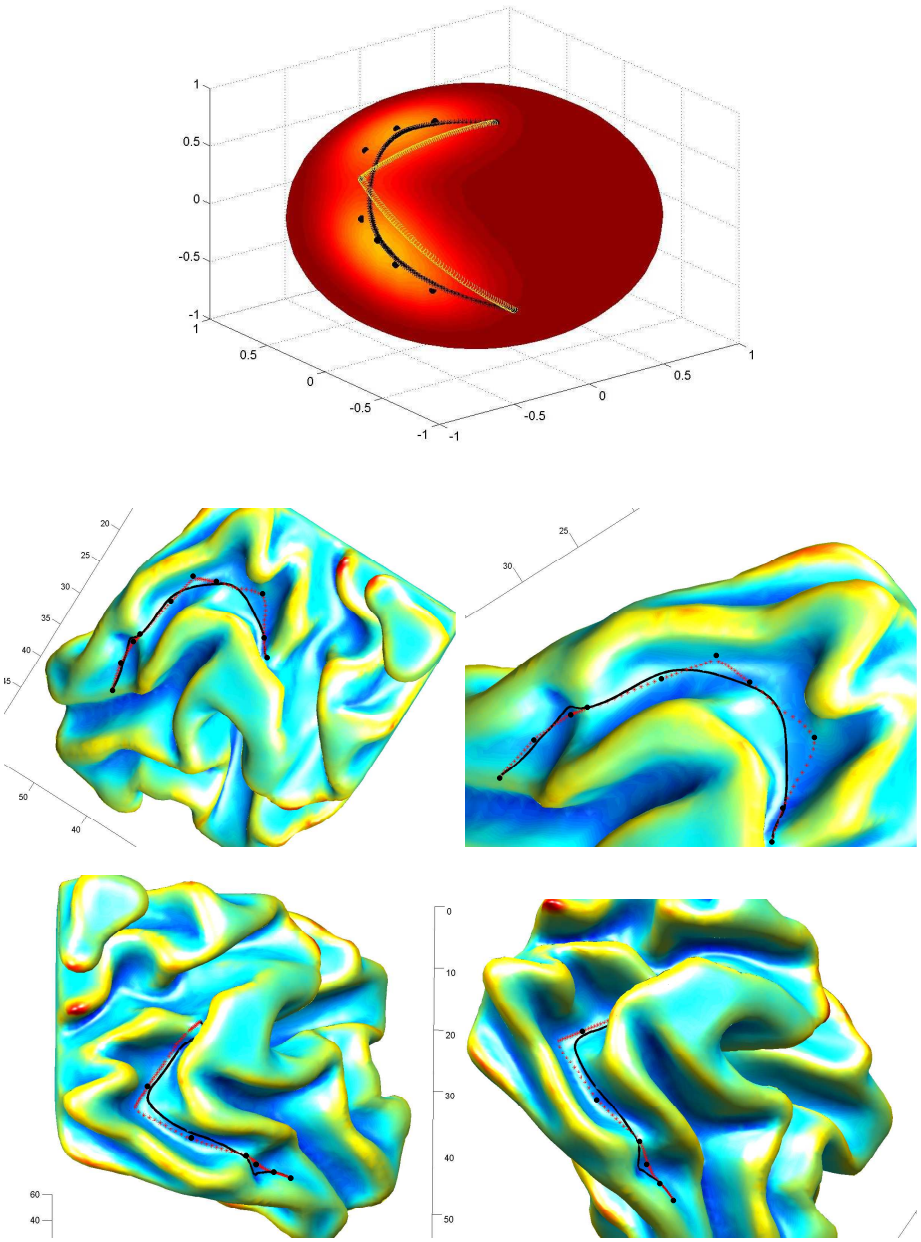

Figure 4: Finding special curves on implicit target surfaces. From an initial curve, adding constraints to the classical harmonic energy, we obtain curves that are attracted to marked points (landmarks). See text for details. *(This is a color figure.)*

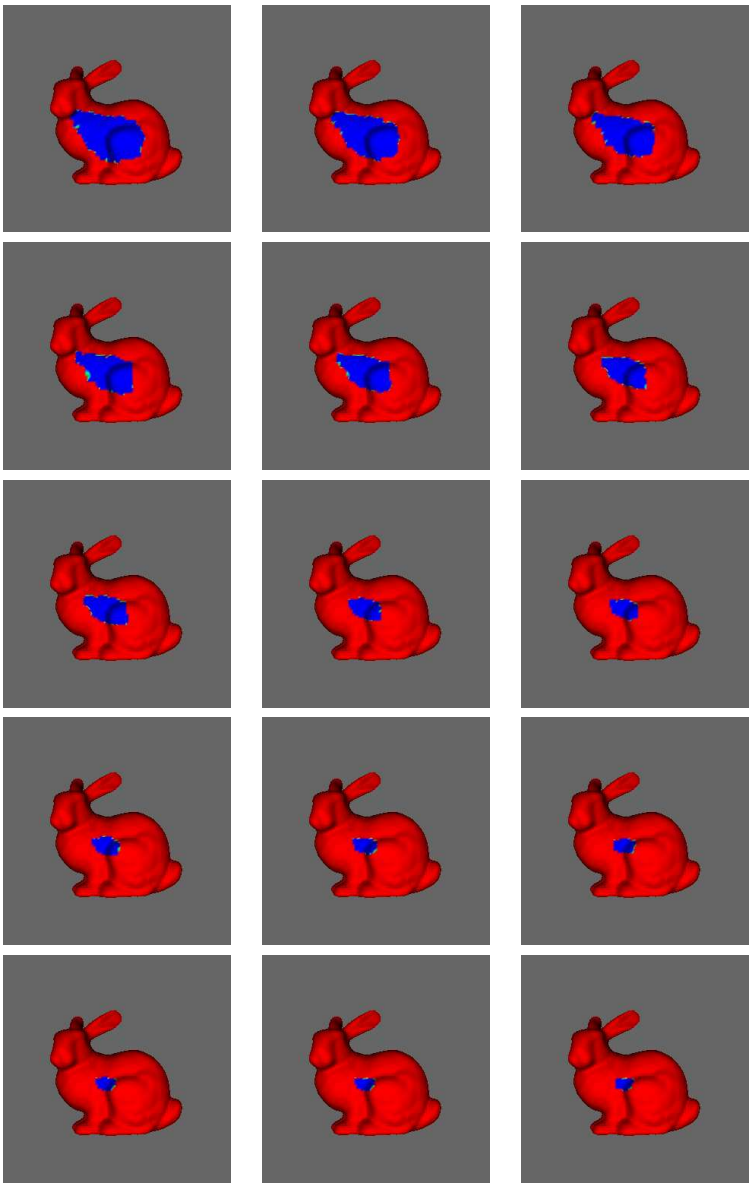

Figure 5: Diffusion of a random map from an implicit torus to the implicit bunny. In blue are marked those points of the bunny's surface pointed to by the map at every instant (the image through the map at each time t of the whole torus). Different figures correspond to increasing instances of the evolution, from top to bottom and left to right. We show the map at 15 of 100 iterations performed on the initial map with a time step of $.01$. We used the 2-harmonic heat flow with adiabatic conditions. *(This is a color figure.)*